Supporting Information

High-efficiency luminescent organic-inorganic hybrid manganese(II) halides applied to X-ray imaging

Haixing Meng, Wenjuan Zhu, Zijian Zhou, Ruyi Zhou, Dong Yan, Qiang Zhao* and Shujuan Liu*

Materials

All raw materials, (methoxymethyl)triphenylphosphonium chloride (99%), (3-methoxybenzyl)triphenylphosphonium chloride (95%), (4-fluorobenzyl)triphenylphosphoniumchloride (95%), isobutyltriphenylphosphonium bromide (98%), (1,3-dioxolan-2-ylmethyl)triphenylphosphonium bromide (97%), manganese(II) bromide tetrahydrate ($MnBr_2 \cdot 4H_2O$, 98%) and manganese(II) chloride tetrahydrate ($MnCl_2 \cdot 4H_2O$, 98%) were purchased from Energy Chemical without further purification.

Characterization

X-ray Diffraction Analysis

Single crystal suitable for single-crystal X-ray diffraction was selected through an optical microscope, the single crystal was put on top of the capillary and then placed on top of the goniometer head. At room temperature, using ω-2θ scanning technology, the single crystal structure diffraction data was collected on the Bruker Smart Apex CCD Diffractometer with graphite-monochromatic Mo-Kα (λ = 0.71073 Å) as the radiation source. The single crystal structure was analyzed and refined by using the direct method and the full small square method F^2 (SHELX-97 software). Powder X-ray diffraction was performed on the X-ray diffractometer D8 Advance A25.

Thermogravimetric Analysis (TGA)

Thermogravimetric analysis is a method of measuring the relationship between the mass of a substance and temperature or time under the control of the program temperature, in order to analyze the thermal stability and thermal decomposition of the material. The experimental data was obtained through the NETZSCH STA-2500 Regulus thermal analyzer under pure nitrogen atmosphere.

Elemental Analysis (EA)

The elemental analysis (C, H) of the manganese(II) halides were conducted by the elemental analyzer model Vario MICRO cube. The elemental analysis results are as follows: $(C_{20}H_{20}OP)_2MnCl_4$ (CP1): Elemental analysis calcd (%): C 59.21, H 4.97; Found: C 59.23, H 4.77. $(C_{26}H_{24}OP)_2MnCl_4$ (CP2): Elemental analysis calcd (%): C 64.81, H 5.02; Found: C 64.71, H 4.96. $(C_{25}H_{21}FP)_2MnCl_4$ (CP3): Elemental analysis calcd (%): C 63.92, H 4.51; Found: C 64.00, H 4.43. $(C_{22}H_{24}P)_2MnBr_4$ (CP4): Elemental analysis calcd (%): C 52.15, H 4.77; Found: C 52.23, H 4.65. $(C_{22}H_{22}O_2P)_2MnBr_4$ (CP5): Elemental analysis calcd (%): C 49.24, H 4.13; Found: C 49.18, H 4.33.

Optical Performance Measurements

Photoluminescence (PL) emission, excitation spectra and time-resolved PL decays were recorded by an Edinburgh FLS-980 spectrophotometer equipped with 450 W xenon lamp source and flash lamp, and the lifetime measurement range is 100 ps-10 s. The photoluminescence quantum yields were measured by Edinburgh FLS-980 with an integrating sphere.

Calculation of X-ray Attenuation Efficiency

In order to obtain the attenuation efficiency (*AE*) of X-ray, we can calculate it by the following formula:

$$AE(\varepsilon,d) = \left(1 - e^{-c(\varepsilon)\rho d}\right)\cdot 100\%$$

The X-ray absorption coefficient (α) is defined as follows: $\alpha = c(\varepsilon) \times \rho$, where *c(ε)* represents the photon cross-section function obtained from the National Institute of Standards and Technology (NIST) XCOM database, while ρ is the scintillator density,

ε is the corresponding photon energy, and d represents the thickness of the scintillator. To calculate the relationship between the scintillator thickness and the X-ray attenuation efficiency, we used 22 keV (the mean and peak value of our X-ray tube) as the photon energy.

Calculation of Steady-state X-ray to Visible Light Conversion Efficiency

In order to standardize and calibrate the light conversion efficiency of scintillators, a commercial LuAG:Ce scintillator was used as a reference standard. To ensure the preciseness of the experiment, our samples and LuAG:Ce were ground into fine powder and prepared into scintillator wafers with same diameter of 1.3 cm and same thickness of 100 μm. Furthermore, we placed our scintillator and the reference scintillator strictly in the same position, and measured their RL spectra under the same conditions. Then, the corresponding photon counting results ($PC_{measured}$) were obtained by integrating the RL spectra. The steady-state X-ray to visible light conversion efficiency is defined as the ratio of the number of emitted photons to the total absorbed X-ray energy. From this point of view, the emitted photons should be normalized to the same X-ray attenuation (100%) using the following equation:

$$PC_{normalized} = \frac{PC_{measured}}{AE(d)}$$

where *AE(d)* represents the X-ray attenuation (%) of the scintillator at a certain thickness. Finally, the light conversion efficiency of our scintillator (*LCE*) were calculated from the following equation:

$$LCE = LY_{LuAG:Ce} \cdot \frac{PC_{normalized}}{PC_{normalized}(LuAG:Ce)}$$

where $LY_{LuAG:Ce}$ in the formula is the known light yield of 22 ± 4 photons/keV for LuAG:Ce, $PC_{normalized}$ and $PC_{normalized}(LuAG:Ce)$ represent the photon counts of our scintillator and LuAG:Ce after normalizing to the corresponding X-ray attenuation, respectively.

X-ray Scintillation Performance Characterizations

The scintillator screen was prepared by mixing finely ground manganese complex and PMMA in a toluene solution in a certain mass ratio, and volatilizing for 12 hours. The

X-ray luminescence spectra were collected by a self-made system, including fiber-coupled fluorescence spectrometer, integrated ball, Mini-X X-ray tube (Ag target, I_{max} = 79 μA, V_{max} = 50 kV) and Complementary Metal Oxide Semiconductor (CMOS) camera. The linear response relationship was mainly obtained through the integration of the RL spectra. X-ray dose rates were tuned by changing the tube current and the tube-to-object. A leakage and low-level X-ray ion chamber dose meter (Radcal Corporation 10X5-180) was used to calibrate the dose rates under different measure conditions. For the light conversion efficiency, a commercially available LuAG:Ce or CsI:Tl scintillator was selected as a comparison. The radiation stability measurement was accomplished with a Mini-X2 X-ray tube (W target, I_{max} = 199 μA, V_{max} = 70 kV). We choose the scintillator with the most suitable thickness for imaging. In this imaging system, X-rays first pass through the object and the internal information of the imaging object was stored on the scintillator screen. Then, the visible light emitted from the scintillator is deflected by a reflector to remove the negative effects caused by direct X-ray radiation to the camera. Finally, the CMOS (Photometrics, Prime 95B) camera collects the visible photons and attain X-ray imaging pictures.

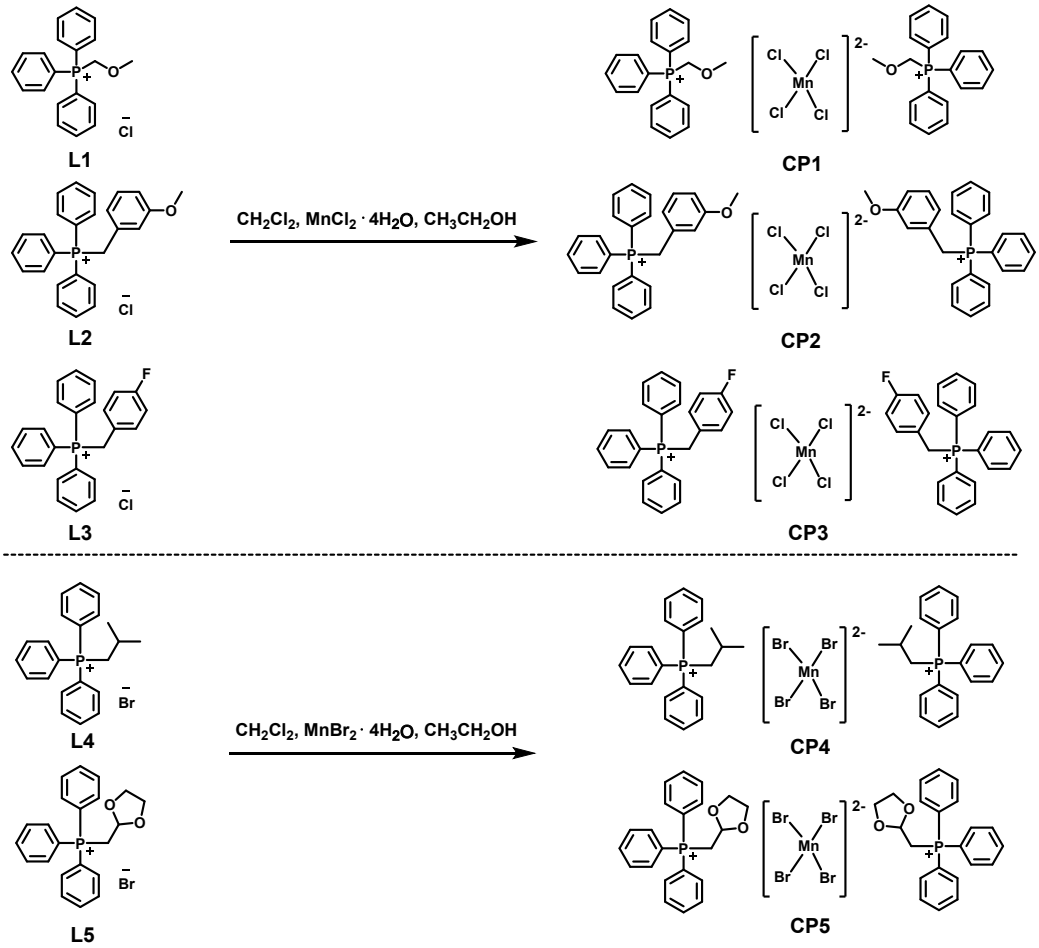

Fig. S1. Synthetic routes of manganese(II) halides CP1-CP5.

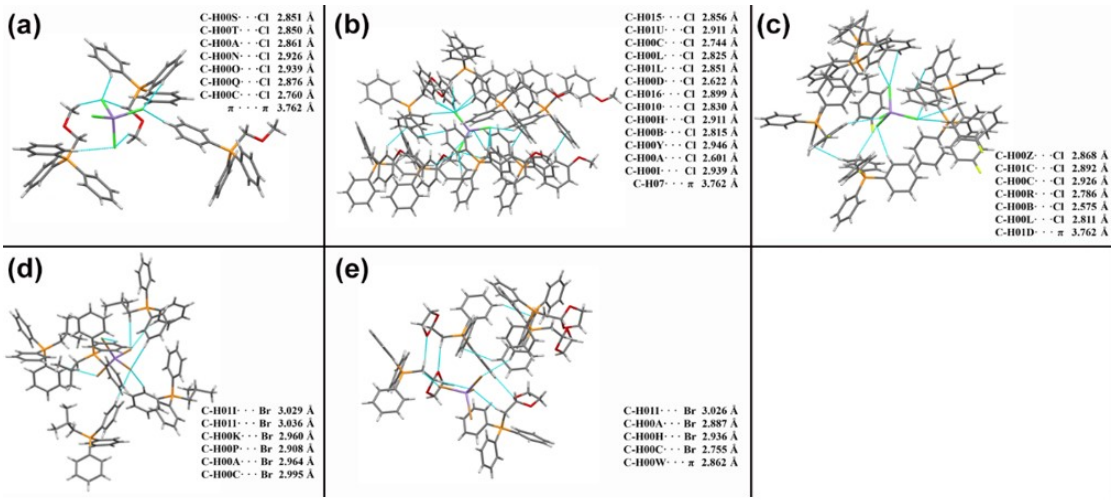

Fig. S2. The intramolecular/intermolecular interactions of CP1-CP5 in crystal structure.

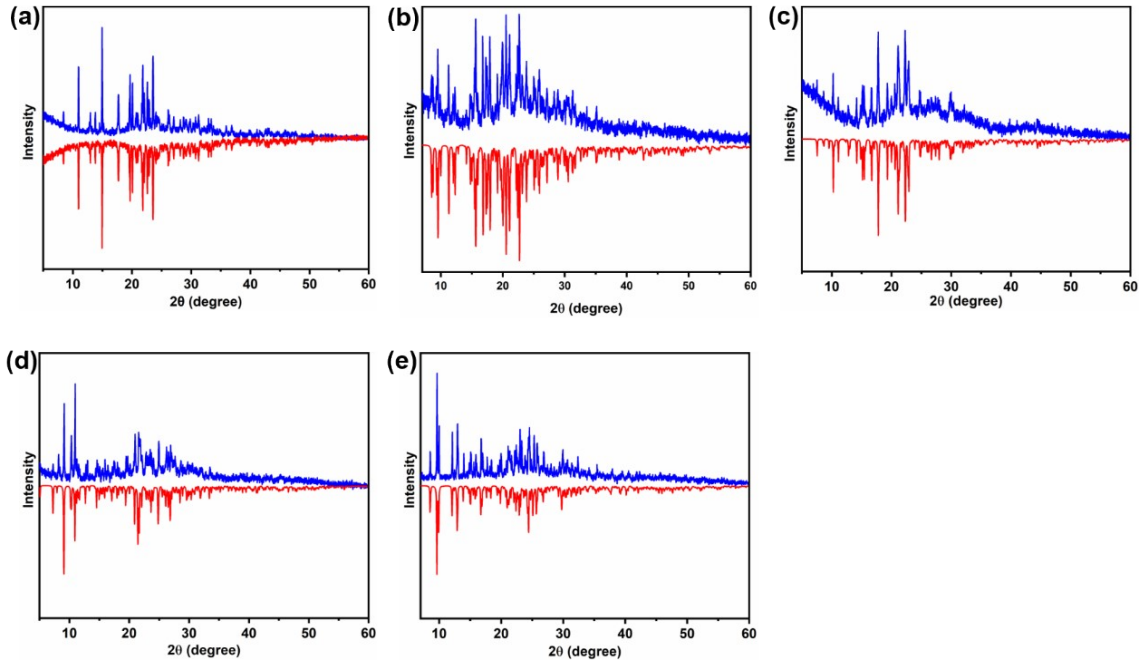

Fig. S3. (a-e) The experimental powder XRD spectra (blue line) of CP1-CP5 compared with the simulated data (red line) from the single crystal structure.

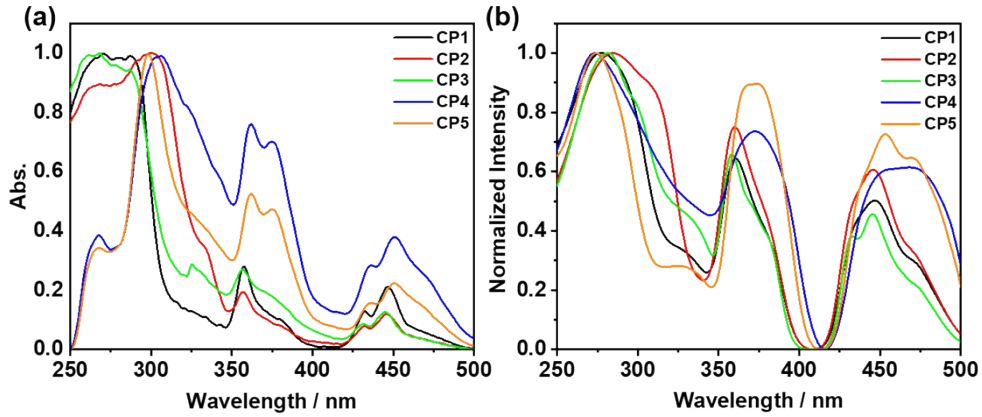

Fig. S4. The absorption spectra (a) and excitation spectra (b) of CP1-CP5 in solid state at 298 K.

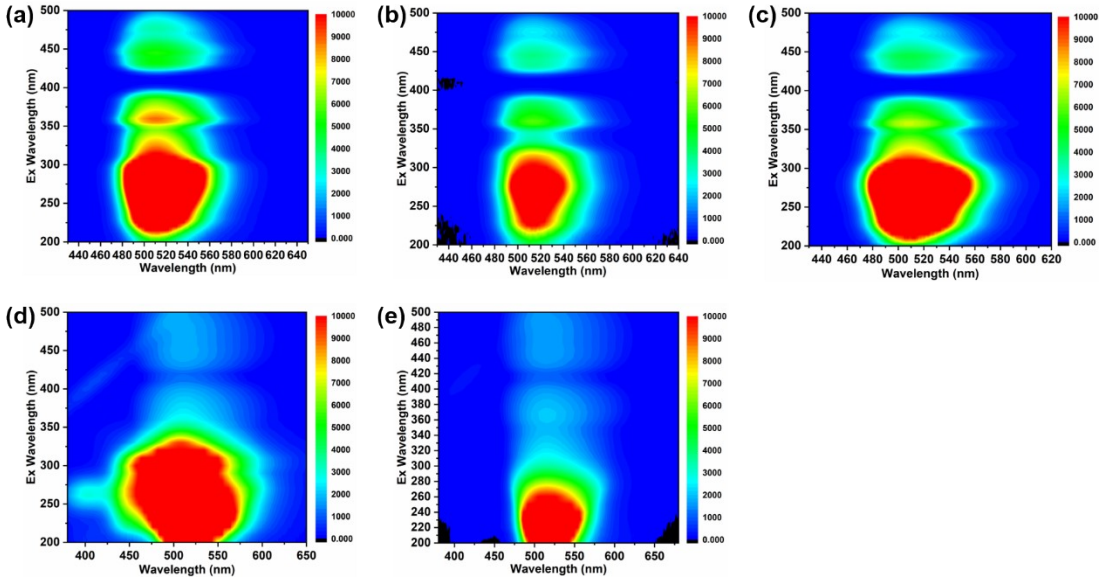

Fig. S5. (a-e) 3D excitation-emission spectra of solid-state CP1-CP5 at 298 K.

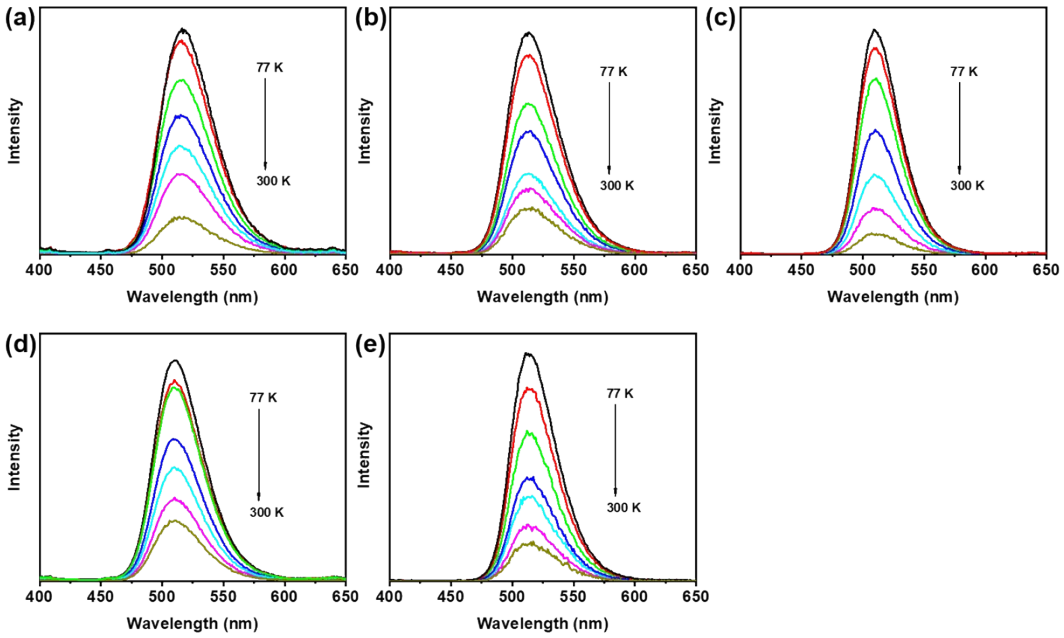

Fig. S6. (a-e) The temperature-dependent emission spectra of CP1-CP5.

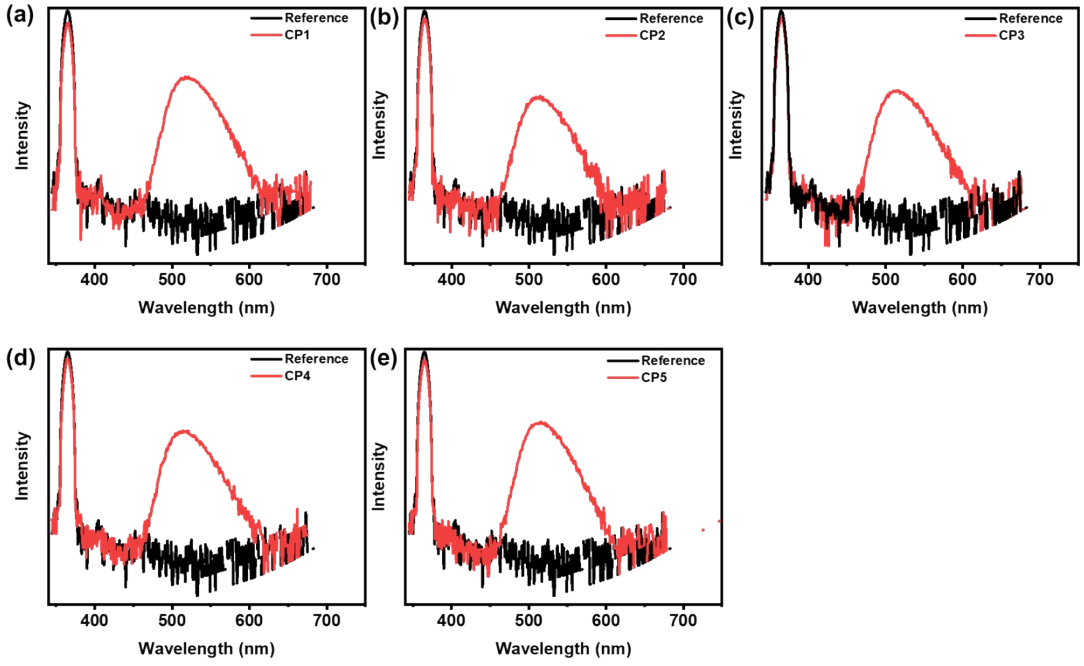

Fig. S7. The PLQY spectra of CP1-CP5 at 298 K.

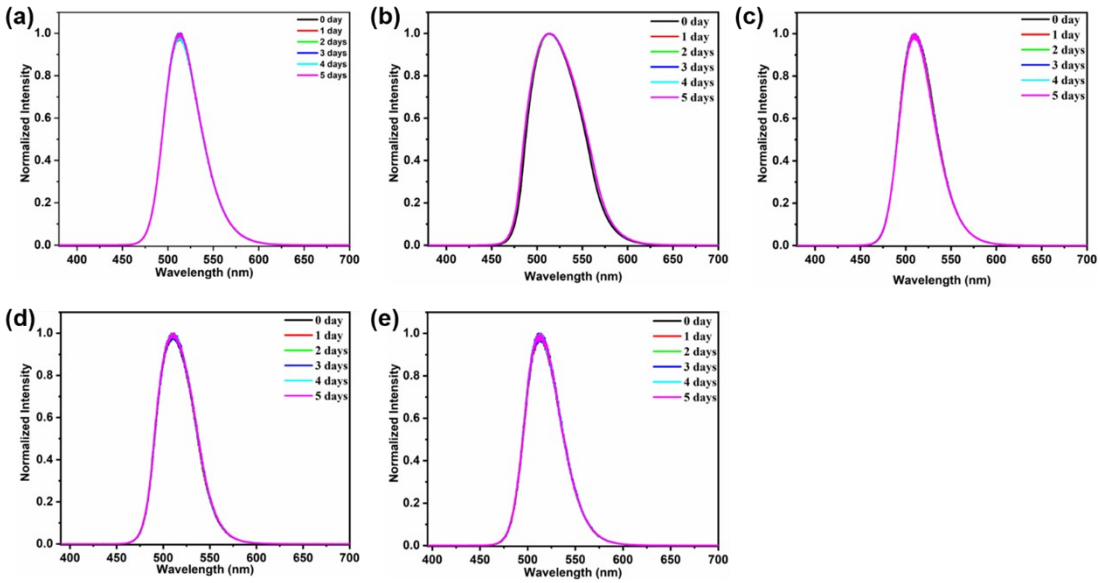

Fig. S8. (a-e) The spectra of CP1-CP5 at ambient conditions for 5 days (25 °C; RH = 50%–60%).

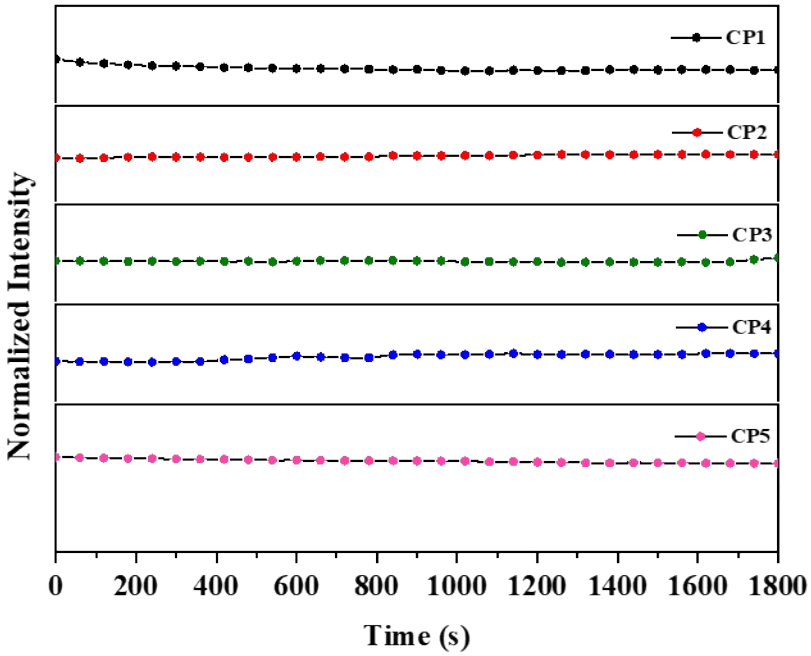

Fig. S9. The PL stability of CP1-CP5 under continuous UV lamp irradiation.

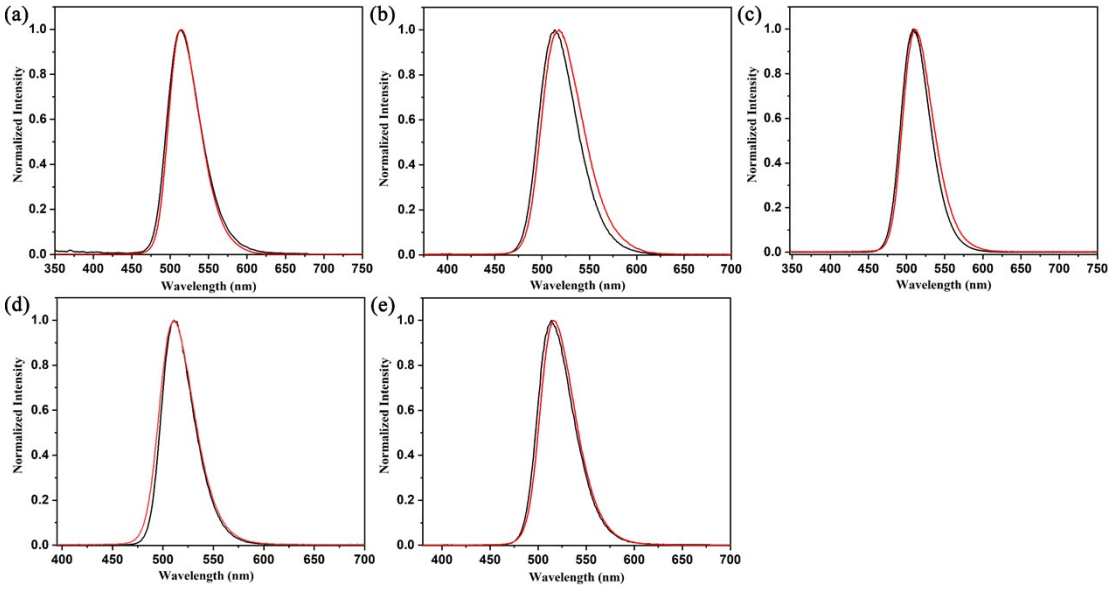

Fig. S10. (a-e) PL spectra and RL spectra of CP1-CP5 (Black line: PL spectra; Red line: RL spectra).

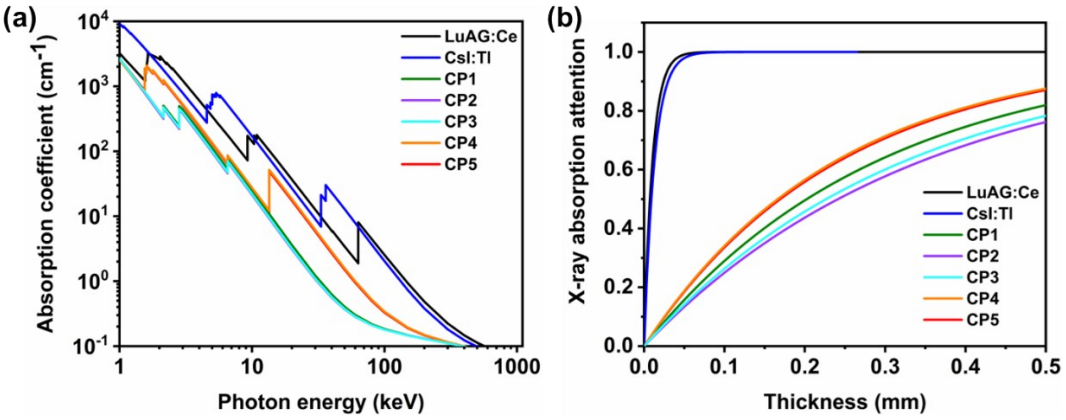

Fig. S11. (a) Absorption coefficients of manganese halides CP1-CP5 and reference scintillator LuAG:Ce and CsI:Tl as a function of photon energy from 1 keV to 1000 keV. (b) X-ray attenuation efficiency of CP1-CP5 and reference scintillator LuAG:Ce and CsI:Tl as a function of film thickness.

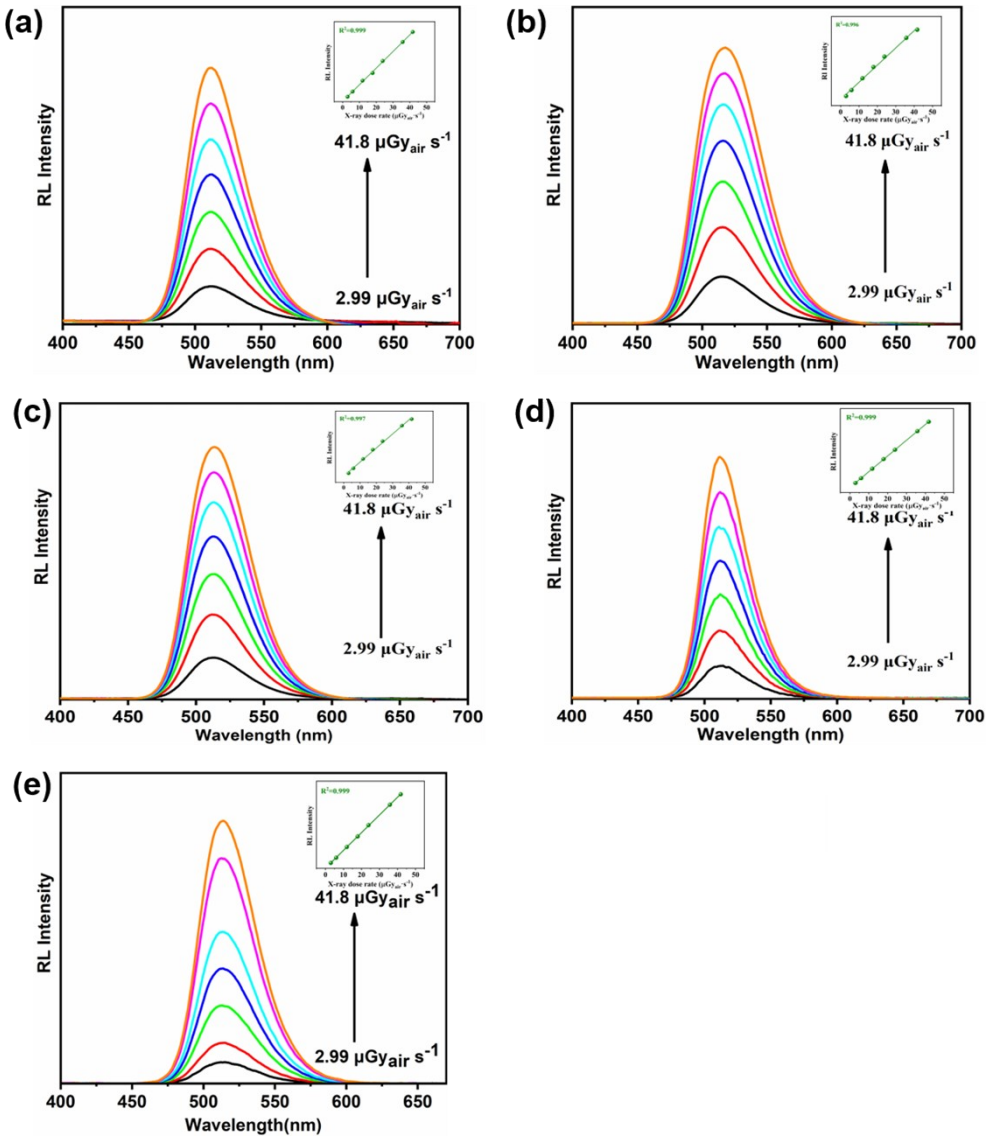

Fig. S12. (a-e) RL spectra of CP1-CP5 under different X-ray radiation dose rates ranging from 2.99 μGy$_{air}$ s^{-1} to 41.8 μGy$_{air}$ s^{-1}, Inset: The linear relationship diagram between RL intensity and different X-ray dose rates.

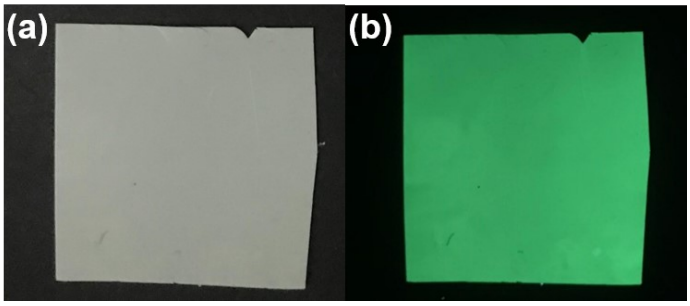

Fig. S13. The photos of scintillation screen (a) and X-ray scintillating screen (b).

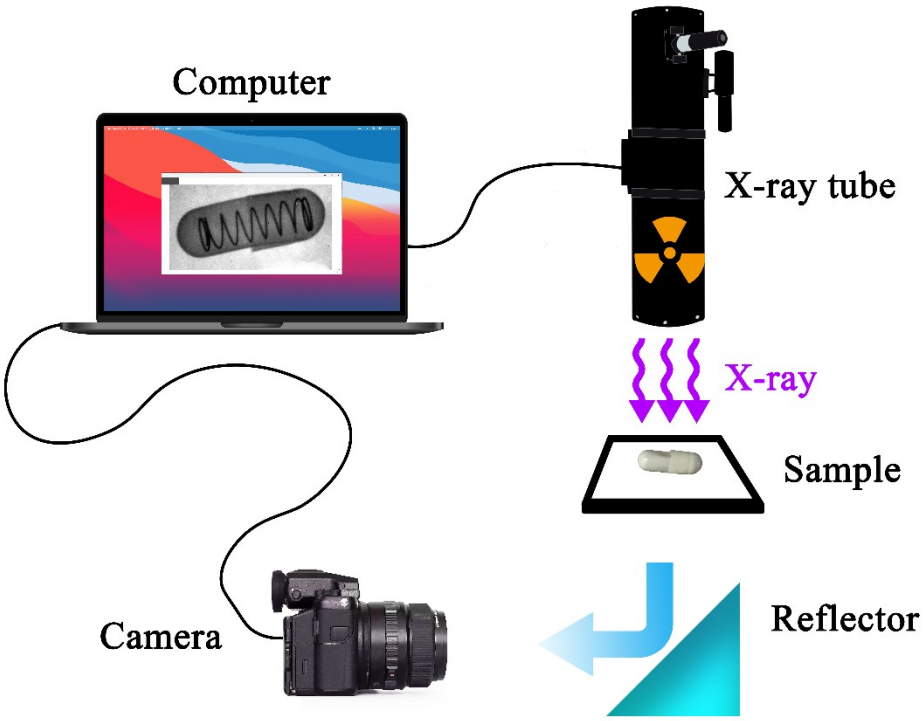

Fig. S14. The spatial distribution diagram of home-made optical imaging system.

Tab. S1. The single crystal X-ray diffraction data of CP1-CP3.

Complex	CP1	CP2	CP3
Empirical Formula	$C_{40}H_{40}Cl_4MnO_2P_2$	$C_{52}H_{48}Cl_4MnO_2P_2$	$C_{50}H_{42}Cl_4MnF_2P_2$
Formula weight	811.40	963.58	939.51
Temperature (K)	295	287	294
Crystal system	monoclinic	monoclinic	orthorhombic
Space group	*C2/c*	*P2₁/c*	*Pbca*
a (Å)	19.0737(15)	19.281(3)	20.7350(19)
b (Å)	16.0861(14)	11.914(2)	18.5345(17)
c (Å)	14.4995(12)	20.833(4)	23.384(2)
α (°)	90	90	90
β (°)	117.915(2)	94.632(5)	90
γ (°)	90	90	90
V (Å^3)	3931.1(6)	4770.2(14)	8986.9(14)
Z	4	4	8
ρ (calcd) (g/cm^3)	1.371	1.342	1.389
F (000)	1676.0	1996.0	3864.0
Reflections collected	23754	38483	76978
Goodness-of-fit on F^2	1.022	1.039	1.009
Final R indexes [$I >= 2\sigma(I)$]	R_1=0.0465, wR_2=0.1072	R_1=0.0610, wR_2=0.1282	R_1=0.0483, wR_2=0.0941
Final R indexes [all data]	R_1=0.0784, wR_2=0.1268	R_1=0.1263, wR_2=0.1588	R_1=0.0939, wR_2=0.1111

Tab. S2. The single crystal X-ray diffraction data of CP4-CP5.

Complex	CP4	CP5
Empirical Formula	$C_{44}H_{48}Br_4MnP_2$	$C_{44}H_{44}Br_4MnO_4P_2$
Formula weight	1013.34	1073.31
Temperature (K)	299	299
Crystal system	orthorhombic	monoclinic
Space group	*Pbca*	$P2_1/n$
a (Å)	17.111(3)	12.214(5)
b (Å)	16.194(3)	18.316(7)
c (Å)	34.656(6)	20.436(8)
α (°)	90	90
β (°)	90	91.498(10)
γ (°)	90	90
V (Å^3)	9603(3)	4570(3)
Z	8	4
ρ (calcd) (g/cm^3)	1.519	1.560
F (000)	4392.0	2140
Reflections collected	81067	27877
Goodness-of-fit on F^2	1.107	1.169
Final R indexes [$I >= 2\sigma(I)$]	R_1=0.0700, wR_2=0.1075	R_1=0.0849, wR_2=0.1730
Final R indexes [all data]	R_1=0.1527, wR_2=0.1310	R_1=0.1529, wR_2=0.2068